Palaeogeography, Palaeoclimatology, Palaeoecology 569 (2021) 110331

Contents lists available at ScienceDirect

Palaeogeography, Palaeoclimatology, Palaeoecology

journal homepage: www.elsevier.com/locate/palaeo

A 14000 year multi-proxy alluvial record of ecotone changes in a Fynbos-Succulent Karoo transition in South Africa

L. Scott [a,*], S. Manzano [b], A.S. Carr [c], C. Cordova [d,e], J. Ochando [f], M.D. Bateman [g], J.S. Carrión [f]

[a] Department of Plant Sciences, University of the Free State, Bloemfontein, South Africa
[b] Plant Conservation Unit, Dept. Biological Sciences, University of Cape Town, HW Pearson Building, Private Bag X3, Rondebosch 7701, South Africa
[c] School of Geography, Geology and the Environment, University of Leicester, University Road, Leicester LE1, 7RH, UK
[d] Department of Geography, Oklahoma State University, Stillwater, OK 74078, USA
[e] Laboratory of Archaeology, Kazan Federal University, Kazan, Tatarstan, Russia
[f] Department of Plant Biology, University of Murcia, Spain
[g] Department of Geography, University of Sheffield, Winter St., Sheffield S10 2TN, UK

ARTICLE INFO

Editor: Paul Hesse

Keywords:
Pollen
Southern Hemisphere
Younger Dryas
OSL
Radiocarbon
Seasonality

ABSTRACT

To address long-standing questions concerning Southern Hemisphere climate dynamics and palaeoecological change in southern Africa, a Late Glacial-Holocene alluvial sediment sequence from the relatively dry interior year-round rainfall zone in South Africa was investigated. The study site borders the Fynbos biome and Succulent Karoo biome ecotone, and comprises a rare stratified sequence of sandy and organic-rich silt deposits, shown to span the last 14,000 years. A high resolution multi-proxy record of ecological change was derived using pollen, phytoliths and organic geochemical analyses. For the period 14–11 ka, significant valley aggradation occurred under relatively drier conditions, followed, during the early and middle Holocene, by alternating phases of humid and dry events with higher stream energy, slower accumulation or subtle seasonality changes. A transition from relatively humid to more arid conditions at 4–3 ka is identified and is consistent in timing with several interior year-round rainfall zone records. Results revealed alternations of fynbos and karroid elements and C_3/C_4 grasses throughout the last fourteen thousand years, but did not suggest large-scale biome shifts. The record joins a growing number of sites contributing to debate over the complex atmospheric-oceanic drivers of palaeoclimate in this region. These data broadly fit to the regional pattern for the southernmost interior of South Africa in showing alternating influences from the westerly winter rain systems in the early Holocene, with a greater contribution from subtropical summer rain system during the middle and later Holocene.

1. Introduction

South Africa occupies an area under the influence of both the southern westerly winter rainfall and the north-eastern subtropical summer rainfall systems of southern Africa (Taljaard, 1966; Tyson and Preston-Whyte, 2000) (Fig. 1). The dynamic transitional zone between these rainfall regimes lies broadly across the boundary between the Eastern and Western Cape Provinces (Fig. 1), generating an essentially year-round rainfall regime, which combined with marked patterns in geological substrate and topography, also produces sharp ecotones between major southern African biomes; namely the Fynbos, Succulent Karoo, Nama Karoo and Albany Thicket Biomes (Mucina and Rutherford, 2006).

It is long-recognised that an understanding of the dynamics of the summer-winter-transitional rainfall zones of southern Africa will inform our wider understanding of Southern Hemisphere climate and biodiversity dynamics (van Zinderen Bakker, 1976; Chase and Meadows, 2007; Chevalier and Chase, 2015). Despite the known challenges of palaeoecological research in these arid to semi-arid environments, there is a steadily growing number of palaeoecological sites from the Cape inland and coastal regions. Notable examples are the pollen records from the Nama Karoo Biome to the north at Blydefontein (Scott et al., 2005, 2012) and isotope, charcoal, pollen, microfauna records from the Albany Thicket and Fynbos Biomes to the south-east and west; viz. Baviaanskloof (Chase et al., 2020), the Cango Valley (Cango Caves and Boomplaas Cave) (Scholtz, 1986; Talma and Vogel, 1992; Thackeray,

* Corresponding author.
E-mail addresses: scottl@ufs.ac.za (L. Scott), saul.manzanorodriguez@uct.ac.za (S. Manzano), asc18@leicester.ac.uk (A.S. Carr), carlos.cordova@okstate.edu (C. Cordova), juan.ochando@um.es (J. Ochando), m.d.bateman@sheffield.ac.uk (M.D. Bateman), carrion@um.es (J.S. Carrión).

https://doi.org/10.1016/j.palaeo.2021.110331
Received 13 October 2020; Received in revised form 23 February 2021; Accepted 23 February 2021
Available online 1 March 2021

1987; Faith et al., 2018) and Seweweekspoort (Chase et al., 2017) (Fig. 1 A). There are also studies on the history of the coastal area in the Fynbos Biome at Norga (Scholtz, 1986); Vankervelsvlei (Quick et al., 2016), Groenvlei (Martin, 1968), Eilandvlei (Quick et al., 2018); Still Bay (Rietvlei) (Quick et al., 2015) and further to the west at Princessvlei (Neumann et al., 2011; Cordova et al., 2019). Along the west coast to the north, there are pollen and isotope records from the fynbos biome in the Cederberg (Scott and Vogel, 2000; Scott and Woodborne, 2007a, 2007b; Quick et al., 2011; Valsecchi et al., 2013; Chase et al., 2015) and from more distant sites like Eksteenfontein in the Succulent Karoo and Pella in the Desert Biome (Scott, 1996; Mucina and Rutherford, 2006; Lim et al., 2016) (Fig. 1A).

Further integrative works i.e., Chase and Meadows (2007), Chase et al. (2013), Chase et al. (2020) and Chase and Quick (2018), have sought to summarize the Quaternary variability in both ocean and atmospheric circulation systems and their impact on southern African climate. Long-term macro-scale climatic influences include a variety of forcing mechanisms e.g., precession or extent of Atlantic sea ice (Berger and Loutre, 1991; Street-Perrott and Perrott, 1993; Nielsen et al., 2004; Fischer et al., 2007; Chase et al., 2013). Recently, Chase and Quick (2018) argued that in contrast to the adjacent interior, the primary driver of climatic change in the southern coastal zone, was the localised coastal influence of the Agulhas Current. Subsequently, Chase et al. (2020) presented further evidence for a coastal-continental interior

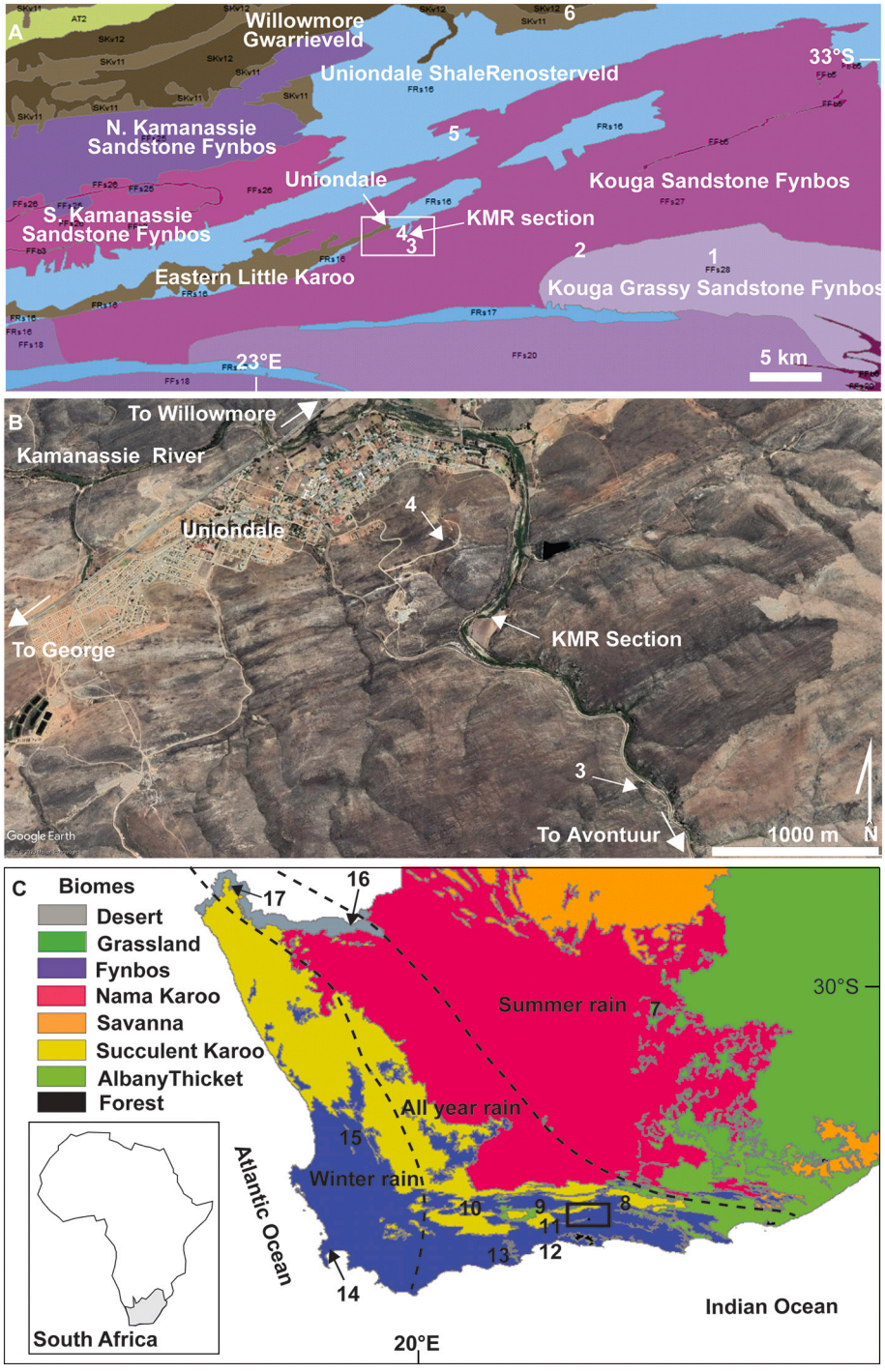

Fig. 1. A. Vegetation types (Mucina and Rutherford, 2006) with numbers 1 to 6 indicating the locations of modern surface pollen samples (see Supplementary Material 1) location of the KMR site (rectangle covers B). B. Locality of the studied KMR Section with the nearest modern samples (3 and 4). C. Biome map (Mucina and Rutherford, 2006) with the study area (rectangle covers A) and key palaeoenvironemenal sites in the region: 7 Blydefontein, 8 Baviaanskloof, 9 Cango Caves/Boomplaas, 10 Seweweekspoort, 11 Norga/Vankersvelsvlei, 12 Groenvlei/Eilandvlei, 13 Rietvlei /Still Bay, 14 Pricess Vlei, 15 Cederberg, 16 Pella, 17 Eksteenfontein.

dichotomy in Holocene climatic trends and time scales. These studies emphasise the need for a detailed network of palaeo-archives to properly untangle regional palaeoclimatic dynamics in this physiographically complex and yet critical climatic/ecological transition zone. The available records need to be better integrated with each other to interrogate such models of ocean and atmospheric circulation patterns.

We have identified several new sites of palaeoecological interest in valleys of the topographically complex eastern Little Karoo between the Great Karoo and southern Cape Fold Belt Mountains near Uniondale (Fig. 1). These comprise extensive (typically 3–10 m thick) alluvial valley-fills containing stratified sequences of organic-rich and sandy fluvial sediment sets within and at the margins of the major mountain fronts. Some of these sequences were exposed by flash flooding in 2007, presenting hitherto under-examined archives of environmental change and landscape response, which can potentially identify environmental changes if studied in sufficient detail over the wider region before they will eventually be lost by future erosion (e.g. Bousman et al., 1988; Cohen and Nanson, 2007). One of these exposed alluvial deposits in the Kamanassie River, henceforth referred to as the KMR sequence (Fig. 1), is the subject of this study. We report the site chronology, as derived with radiocarbon and optically stimulated luminescence (OSL) dating, as well as a complete suite of geochemical, phytolith and palynological data. We view the results in relation to the current vegetation types and ecotones in the region and their pollen production in the Succulent Karoo and Fynbos Biomes (Fig. 1) and compare the new results to the nearest key records to understand the local processes in the formation of the KMR site.

2. Setting

The KMR study site (Fig. 1) is surrounded by areas experiencing semi-arid to sub-humid climates with a suite of geological substrates, resulting in complex biome and vegetation patterns (Fig. 1). The area lies within the all year rainfall region (Taljaard, 1966; Tyson and Preston-Whyte, 2000) receiving ~615 mm rain annually, with slightly lower precipitation during winters than autumns and springs (Mucina and Rutherford, 2006) and with occasional frost in winter (~13 days per year). The mean annual temperature is 15.8 ^{o} C (Tyson and Preston-Whyte, 2000).

The studied alluvial deposits lie at ~870 m altitude, in the Fynbos Biome in the Eastern Fynbos Renosterveld Bioregion (F06) (Mucina and Rutherford, 2006) (Fig. 1) (−33.66561 S, 23.1362 E). They have formed as a valley fill in the Kamanassie River. The catchment of this drainage line starts in fynbos and runs towards more karroid vegetation before eventually turning west towards the Gourits River (Fig. 1 A, B. and C.). The site is bordered to the north by Uniondale Shale Renosterveld and to the south by the montane Kouga Sandstone Fynbos. To the west and north patches of Eastern Little Karoo belonging to the Succulent Karoo Biome occur immediately west of the site and further to the north several kilometres away (Mucina and Rutherford, 2006).

In view of this setting special consideration in interpretations must be given to fluvial transport of organic matter and microscopic material, including pollen, phytoliths and organic debris, which are not necessarily of local origin. However, they are likely derived from within the relatively small Kamanassie River catchment within the Kouga Mountains south of Uniondale. Flood events, fluvial transport, standing water phases, fire and rainfall seasonality all potentially play a role in the deposition and preservation of the organic material relating to past environments of the area.

3. Methods

Samples were recovered directly from the exposed face of the deposit. The same sampled materials were utilised for geochemical, phytolith and pollen analyses, with exceptions depending on the productivity of different proxy types, or the need for specific focus on a particular proxy. The site stratigraphy was logged in detail and 61 samples obtained for analysis indicated in Fig. 2A and a photograph showing the general nature of the section appear in Fig. 2B.

3.1. Dating

Two laboratories, viz., ^{14}Chrono at Queen's University, Belfast and the Accelerator Mass Spectrometry Laboratory at the University of Arizona, Tucson, provided eleven AMS dates for the sequence (two from the east section (Site 1) and nine from the main section (Site 2). They comprised one ^{14}C analysis on bulk organic matter sample, three on pollen extractions and seven on charcoal samples (Table 1). Additionally, optically stimulated luminescence (OSL) ages for three sandy layers using coarse grained quartz, were undertaken at the Sheffield University luminescence laboratory, one from Site 1 and two from Site 2 (see Table 2 and Supplementary Material 1 for more on the OSL dating methods).

3.2. Biogeochemistry

Forty samples were analysed for their Total Nitrogen (TN), Total Organic Carbon (TOC) contents and their $\delta^{13}C_{TOC}$ values to investigate the organic matter composition. To account for the presence of geogenic carbon (carbonate), samples were analysed with (TOC and $\delta^{13}C_{TOC}$) and without (TN) acid treatment. The acid-insoluble residue (TOC) is considered the best representation of the organic carbon present in the sediments and the carbon isotope composition ($\delta^{13}C_{TOC}$) was obtained from this material (See Supplementary Material 1 for methods).

3.3. Microfossil extraction

For investigation of the vegetation history, residues for pollen, non-pollen palynomorphs (NPPs) and phytolith analysis were prepared using standard extraction methods (Faegri and Iversen, 1989), including sodium polytungstate heavy liquid separation (specific gravity 2.3) (Munsterman and Kerstholt, 1996). The microscope slides were mounted in glycerine-jelly and duplicates used for phytolith identification and palynology.

3.4. Phytoliths

A minimum of 300 phytoliths were counted on each slide and phytolith concentration was calculated using *Lycopodium* marker spores (Stockmarr, 1971). Phytolith counts were divided into graminoid and non-graminoid, excluding those that could not be assigned to any group. The classification of phytoliths follows a modified version of previous research in the region (see Supplementary Material 1, Figs. S2&3 for more on methods and classification). Using different phytolith groups and their taxonomic associations, several ratios provide a basis for characterizing vegetation communities along with pollen. The non-graminoid-to-graminoid ratio represents the proportions of plants that do not belong to grass-like plants and provides an idea of closed shrub canopy versus open grassy spaces. Additionally, the Poaceae-Restionaceae ratio, suggests the presence of restioid fynbos.

The grass silica short cell phytolith (GSSC) ratios indicate the relative abundance of C_3 and C_4 grasses. The C_3/C_4 ratio was obtained by dividing the sum of C_3-diagnostic GSSC by the sum of all C_4-diagnostic GSSC. As C_3 grasses are abundant in the winter-rainfall zone of South Africa (Vogel et al., 1978), a mirror ratio, the C_4/C_3x100 GSSC ratio, is used to more clearly visualise the representation of C_4 grass.

3.5. Paleofire proxies

Burned Poaceae phytoliths, presented here as percent of the total Poaceae phytoliths, provide a proxy for grass fires (as opposed to overall fires as indicated by microscopic charcoal; Cordova et al., 2019). Two

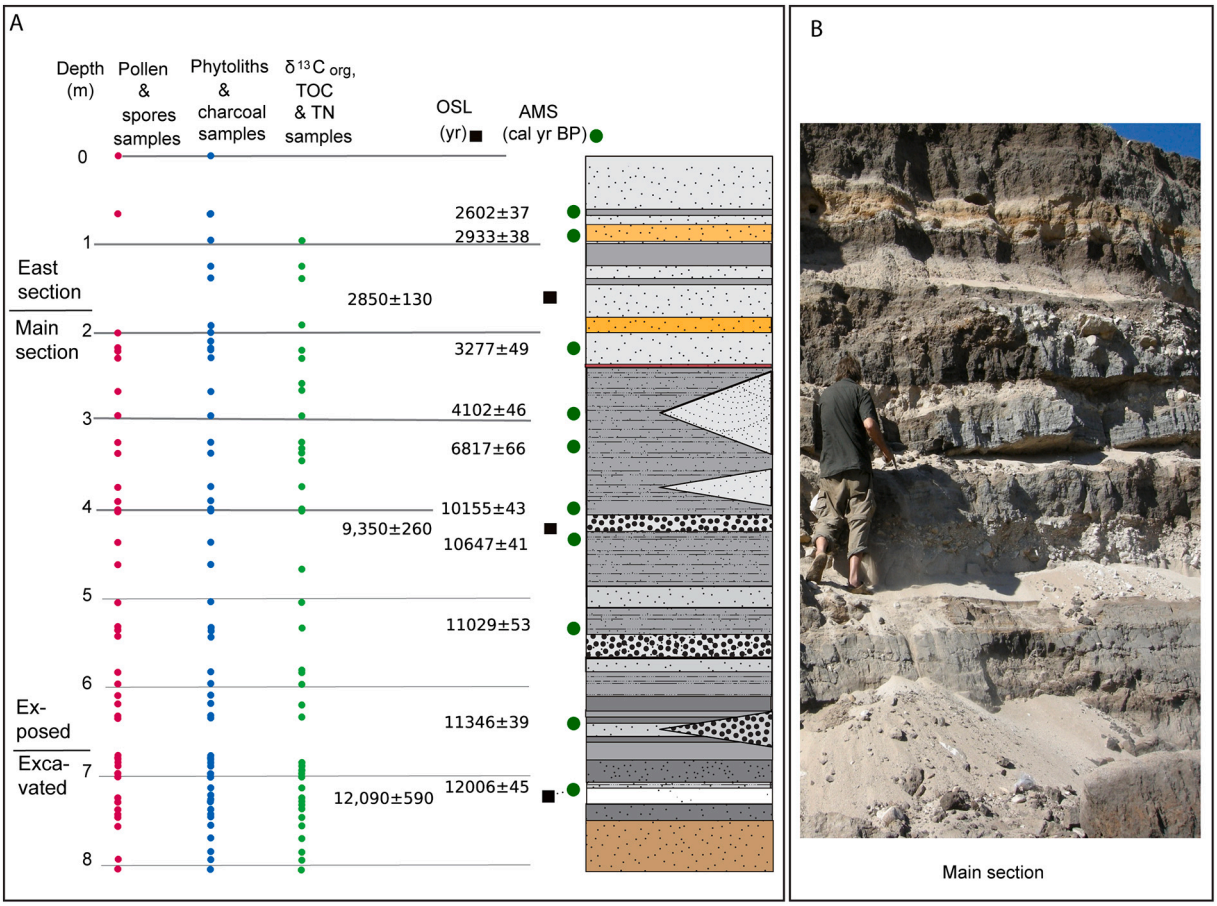

Fig. 2. A. Combined lithological profile of the eastern and main sections. Dots on the left indicate sample positions, of which not all levels were necessarily productive. B. View of the main section with M. Wessels standing at the c. 5.8 m level.

different methods of microscopic charcoal estimation were used during the phytolith and palynological analyses, with one presented here as counts per mm^2 and the other as counts per gram following the addition of spikes of the same *Lycopodium* spores (Stockmarr, 1971) used for concentration estimates in the palynological study (see *Palynology* below and in the Supplementary Material 1).

3.6. Palynology

A minimum of 300 pollen grains from terrestrial plants, plus, aquatics, spores and non-pollen palynomorphs (NPPs including fungal spores and algae) was identified from forty-four productive layers (usually the grey-brown sands with organic material). The light-coloured coarse-grained sands and gravels preserved insufficient pollen. Pollen zones I-V were obtained by CONISS (Grimm, 2011) based on the terrestrial taxa.

Modern surface samples were analysed to assess the modern pollen production for both fynbos and karroid vegetation types (Mucina and Rutherford, 2006) (Fig. 1). Six modern surface-soil samples from near the site and in two transects of ~30 km in different directions away to the south-east along the Kouga Mountains and north-east towards Willowmore, were collected (Fig. 1B) (see Supplementary Material 1 for details and results).

4. Results

4.1. Description of the sequence of deposits

The sequence comprises of a series of distinct, alternating sedimentary units of organic, fine-grained wetland, to coarse-grained sandy and mineral-rich gravelly layers (Fig. 2A, Table 1).

4.2. Dating

The radiocarbon dating results are presented in Table 2 and OSL sample list and results in Tables 3 and 4 respectively. The resulting age model obtained using Bacon and the SHcal13 curve (Blaauw and Christen, 2011; Hogg et al., 2013) is shown in Fig. 3. Because the calibrated radiocarbon ages are expressed as cal yr BP and the OSL as years, ages in subsequent plots of proxy data are expressed as modelled age (yr).

The radiocarbon chronology of the eight-meter KMR sequence is reasonably well supported by the three OSL ages, showing that deposition started around 14,000 years ago before the Younger Dryas (YD). The age-depth model suggests varying sedimentation rates with faster accumulation, implying phases of marked valley fill aggradation from 14,000 to 11,000 years ago and between 4000 and 3000 years ago, with slower accumulation between 7000 and 4000 years ago and during the last 2500 years. The latter phases also have low proxy sample resolution due to their low organic contents.

4.3. Geochemistry

The total organic carbon content is highly variable, ranging from 0.1 to 5.2% (Fig. 4A) (Supplementary Material 2). Although obviously inorganic sand layers were not sampled for organic geochemical analysis, the down-section variation in TOC does largely track the sedimentary facies within the section, with the highest TOC values generally

Table 1
KMR profile description.

KMR sections	Depth (cm)	Description
East	0–180	Organic rich silts/fine sands with rootlets, prominent more organic layers at c. 65, 95, 126 and 135 cm (OSL 2.8 ka, 165 cm)
Main	180–200	Iron stained, coarse sands that pinch out laterally
	200–230	Dark silts below prominent iron stained layer
	235	Prominent reddish sands
	240–405	Laminated grey/black silty sands, rich in organic matter with lenses of coarse sands/gravel and some-pebbles that pinch in and out with some vestiges of bedding that can be traced laterally but tend to pinch out
	405–423	Pebble layer (top is the datum) (OSL 9.4 ka, 4.2 cm)
	425–486	Laminated grey/black silty sands, rich in organic matter
	486–510	Clean (inorganic), coarse sand/some gravel
	510–540	Laminated grey/black silty sands, rich in organic matter, gravel and coarse sand
	540–568	Coarse, quartz-rich laminated sands
	568–583	Grey/brown laminated organic-rich silts, some reddish staining
	583–610	Prominent black silts rich in organic matter
	610–624	Grey/brown laminated organic-rich silts, some reddish staining
	624–665	Grey/brown laminated organic rich silts, some reddish staining above black organic rich clays and coarse sands with a gravel lens that pinches out laterally
	665–685	Coarse grey/brown sand grading downwards over 2–3 cm to grey/black sands
	685–705	Grey/black coarse sands
	710	Dark brown silty fine sands
	712–730	Orange mottled, fine sands (OSL 12.1 ka, 722 cm)
	730–752	Black, water-saturated sands
	752–806	Brown mottled coarse sands

Table 2
Radiocarbon dates from the KMR Section.

Sample ID	Material	Age (yr BP)	Error (yr)	Depth (cm)	Cal yr BP (2 sigma ranges)	$\delta^{13}C_{org}$ (‰)
UBA-20534	Pollen	2583	37	65	2471-2602-2747	−26.3
UBA-20533	Pollen	2960	38	95	2925-2933-3168	−21.6
AA90910	Charcoal	3123	49	220	3141-3277-3391	−26.7
AA90909	Charcoal	3800	46	295	3963-4102-4247	−26.5
UBA-20532	Pollen	6030	66	325	6659-6817-6984	−27.3
UBA-18270	Charcoal	9060	43	400	10121-10155-10246	−28.5
UBA-20337	Charcoal	9473	41	430	10541-10647-10754	−25.7
AA90133	Organics	9736	53	463	11063-11029-11223	−26.3
UBA-20338	Charcoal	9865	43	537	11170-11225-11311	−29.0
UBA-18269	Charcoal	9977	39	640	11228-11346-11411	−25.7
UBA-18271	Charcoal	10,311	46	715	11763-12006-12155	−19.8

associated with dark coloured silts and silty sands (e.g. 4.68, 5.35, 6.87 m, associated ages of 11 ka, 11.3 ka and 12 ka). TN closely tracks TOC (Pearson's $R = 0.99$), suggesting the former is most likely organic N. The TOC/TN ratio ranges between 36 and 7 (Fig. 4B), but largely falls in the range 10–25 (mean = 21 ± 5). The two outlier TOC/TN values at 9.0 and 11.5 ka are associated with TN contents <0.03% and are potentially impacted by measurement imprecision at such low N contents. Except for these two outlier values, there are no trends in TOC/TN through the sequence; the Late Holocene (2.9–3.8 ka) mean TOC/TN (21 ± 4) is identical to that of the Late Glacial (11.5–13.8 ka; 20 ± 4). In the more sporadically preserved early to mid-Holocene section (11.3–6.5 ka) the average ratio is marginally higher (25 ± 5), but the significance of this is hard to evaluate given the limited number of samples.

Table 3
OSL sample list for KMR section.

Field code	Sample code	Depth from surface (m)
KMR10/1/3 Site 1	Shfd10083	1.65
KMR10/1/1 Site 2	Shfd10081	4.20
KMR10/1/2 Site 2	Shfd10082	7.22

The $\delta^{13}C_{TOC}$ ranges between −25.6 and − 21.3‰ (Fig. 4C) with some clear trends apparent. From a sequence maximum of −21.3‰ at the base of the sequence (13.8 ka), $\delta^{13}C_{TOC}$ declines steadily (with a brief rise to −21.8‰ at 12.1 ka) to −25‰ at 11.0 ka, whereupon it remains relatively stable to 6.5 ka (−24.4 ± 0.4‰). In the late Holocene section (3.8–3.0 ka) $\delta^{13}C_{TOC}$ is higher than the early to mid-Holocene and is clustered at −23.7 ± 0.9‰. The precise timing of this late Holocene shift to higher $\delta^{13}C_{TOC}$ is difficult to determine given the limited number of mid to late Holocene samples, although the $\delta^{13}C_{TOC}$ of the immediately subjacent sample at ~4.2 ka is lower (−25.6‰) than those above it.

4.4. Phytoliths

The distribution of silica phytolith morphotypes varies considerably, but they are best preserved in zones 1, 2 and 4 (Figs. 5 and 6) of five zones (Supplementary Material 2).

Although with relatively low counts, Phytolith zone 1 (14–12.9 ka) shows a clear dominance of non-graminoids over graminoids (Fig. 5). For the latter, the incidence of Poaceae is lower than Restionaceae and unclassified graminoids. Poaceae phytoliths are highly variable through the zone, and the percent of burnt phytoliths is low (Fig. 6). GSSC show approximately equal abundances of C_3 and C_4 grasses, with the latter always exclusively the Chloridoideae (Fig. 7).

Phytolith zone 2 (12.9–10.6 ka) shows a gradual increase of graminoids over non-graminoids (Figs. 6 and 7). Within the graminoids, Poaceae increase relative to Restionaceae phytoliths (Fig. 5). Within Poaceae short cells become increasingly more abundant towards 11 ka, suggesting perhaps better preservation or higher phytolith input by wind (Fig. 6). Burnt grass phytoliths also increase towards 11 ka, reaching their highest abundance for the sequence, and they suggest an increase of grass fires. In the GSSC, the proportion of C_3 vs. C_4 remains the same as phytolith zone 1, except for a single-sample peak in C_4 and a relative increase in Panicoideae diagnostic GSSC at c. 12 ka (Fig. 7).

Phytolith zone 3 (8.2–3 ka) is associated with few samples that preserve plant silica, probably reflecting the coarser sediment texture. However, it shows a general distribution of phytolith groups like the top of zone 2, with graminoids dominating over non-graminoids, and Poaceae dominant over Restionaceae. Similarly, the proportions of Poaceae morphotypes remain relatively unchanged, with short cells dominating alongside a marked reduction in the percentage of burnt grass phytoliths (Fig. 6). The GSSC also show notable changes across the zone (Fig. 7). Before 6 ka C_3-diagnostic GSSC dominate, while among the C_4 the Panicoideae remain significant. After 6 ka, the proportions of C_3 decline in favour of C_4, and among the latter Chloridoideae becomes dominant over Panicoideae.

Phytolith zone 4 (3–1.9 ka) shows a moderate incidence of non-graminoids over graminoids, and of Restionaceae over Poacaeae (Fig. 5). Among Poaceae phytoliths, dominance fluctuates between short cells and bulliforms, while the percent of burnt grass phytoliths

Table 4
OSL related data for KMR section.

Depth (m)	Water content (%)	K (%)	U (ppm)	Th (ppm)	Cosmic dose rate (Gy kyr^{-1})	Total dose rate (Gy kyr^{-1})	D_e (Gy)	Age (C.E.)
1.65	0.1	0.16	0.98	1.93	0.18 ± 0.01	0.71 ± 0.03	2.04 ± 0.05	2890 ± 140
4.20	0.2	0.35	1.00	4.06	0.13 ± 0.01	1.00 ± 0.04	9.36 ± 0.26	9360 ± 440
7.22	11.1	0.13	0.57	3.69	0.12 ± 0.01	0.60 ± 0.02	7.26 ± 0.25	12,030 ± 590

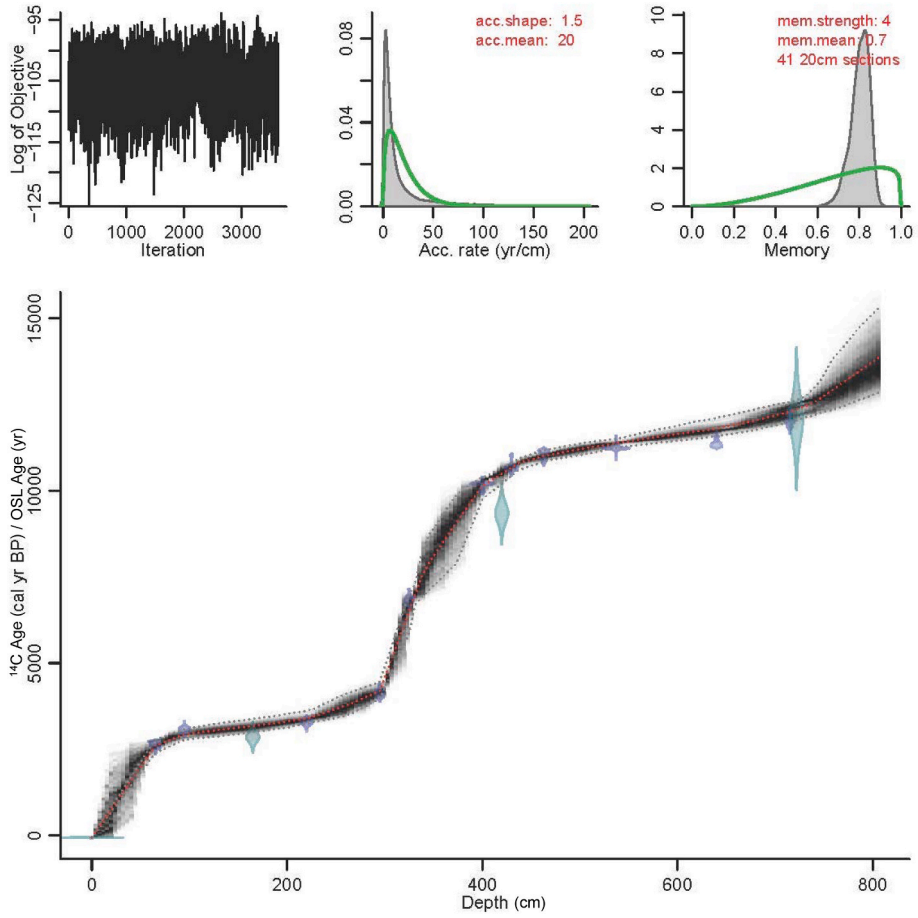

Fig. 3. Bacon age model using Blaauw and Christen (2011). Radiocarbon dates: light blue; OSL dates: light blue-green. (For interpretation of the references to colour in this figure legend, the reader is referred to the web version of this article.)

increases. The proportions of C_3 and C_4-diagnostic GSSC indicates an increase in C_3, while within the C_4-diagnostic GSSC the proportions of Panicoideae dominate over Chloridoideae at times.

Phytolith zone 5 (from 1.9 ka onwards) consists of two samples. Notably the proportions of graminoids and Poaceae are higher in the top sample, (Fig. 5), with bulliforms dominating among the Poaceae (Fig. 6). The top sample shows a codominance between C_3 and C_4, with the latter dominated entirely by Panicoideae.

4.5. Paleofire proxies

The results of the two methods of micro-charcoal determination record the same trend, with an apparent peak in fire at ~11.5 ka, lower intensity of fire until the late Holocene, followed by a second peak at c. 4 ka (Fig. 8 and Fig. S4 in Supplemetary Material 1 for size classes).

4.6. Palynology

Pollen concentrations in KMR section were highly variable and highest pollen concentrations occurred in the samples at c. 12 ka (Fig. 8) (Supplementary Material 2).

Pollen characteristic of fynbos vegetation, as well as Asteraceae, Poaceae and succulent pollen groups are prominent throughout the sequence. Variability across numerous individual pollen types is high at some levels in the sequence. Despite distinctive changes in the individual pollen types, the relative abundance of these groups is largely consistent, suggesting relatively subtle changes in vegetation over the studied interval (Figs. 9 and 10). Apart from the regional pollen (Fig. 9), we observe variations in other palynomorphs (Fig. 10) of aquatic pollen types, cryptogam spores, fungal spores and algae (local palynomorphs and NPPs).

The diagrams of arboreal and non-arboreal pollen show sharp relatively short-term oscillations, but long-term or developmental trends are difficult to visualise. The zonation is therefore based on the CONISS results: I) 13.9–2.1 ka, II) 12.1–8.3 ka, III) 8.5–4 ka, IV) 4–3 ka and V) 3 ka-present (Fig. 9B).

Pollen zone I (13.9–12.1 ka) starts with prominent Asteracaeae (undifferentiated) peak accompanied by an initial prominence of *Stoebe* type at 13.9 ka. It is otherwise associated mainly with grasses (Poaceae), some trees (*Euclea sp.*) and some fynbos shrubs (Ericaceae, *Passerina* sp. and Restionaceae). The Younger Dryas (YD) period (c. 12.8–11.5 ka) spans the transition between Pollen zones I and II (12.1–8.3 ka). Pollen

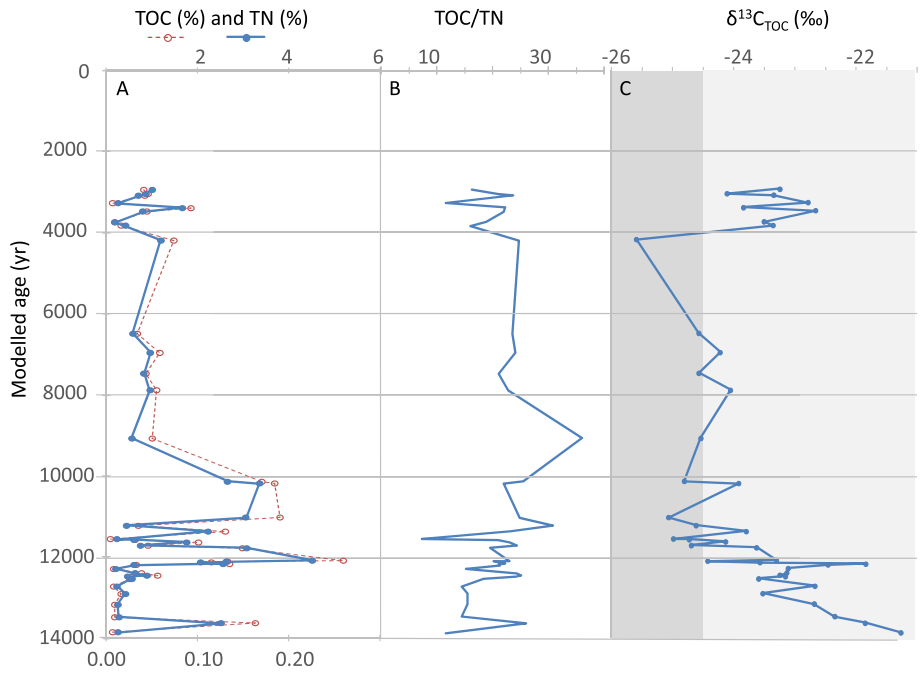

Fig. 4. A. TOC (red/dashed, top scale) and TN (blue, bottom scale). B. TOC/TN. C. Down-section trends in $\delta^{13}C_{TOC}$. Dark and light shades indicate measured ranges of typical soil $\delta^{13}C_{TOC}$ from the Fynbos and Succulent Karoo Biomes respectively (Carr et al., 2021). (For interpretation of the references to colour in this figure legend, the reader is referred to the web version of this article.)

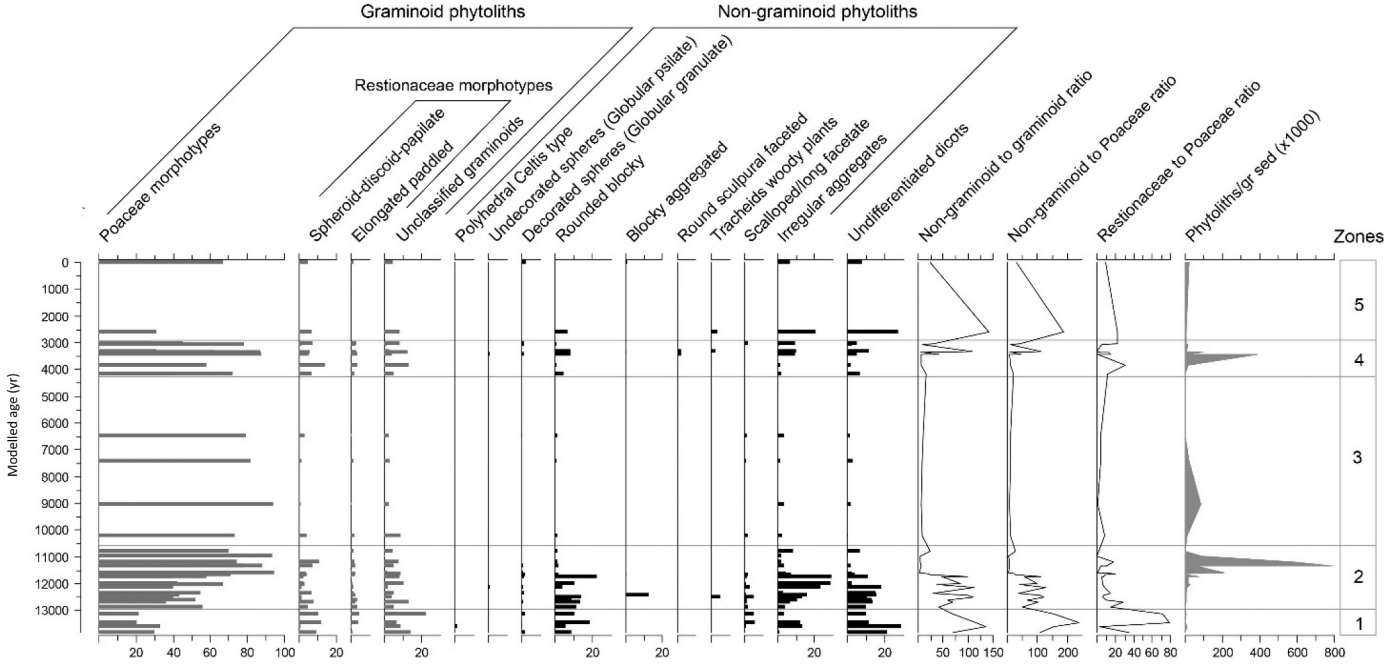

Fig. 5. Phytolith groups, summary and ratios.

from the base of the YD (Pollen zone I) continues to show relatively high proportions of Asteraceae (undifferentiated), while some woody plant pollen like *Euclea*, *Clutia* and *Buddleja* increase, together with Restionaceae and some fynbos elements. The woody elements decline c. 11.7 ka and some of the fynbos, e.g., Ericaceae, *Passerina* sp. and *Cliffortia* sp. continues to be present in fair numbers in Pollen zone II (Fig. 9 A). Grass and Asteraceae pollen (including varying numbers of *Stoebe* type) are prominent while different fynbos types persist. Of the fynbos types, Restionaceae pollen shows a strong decline c. 11 ka, after which succulents (Aizoaceae type and *Ruschia*) peak c. 10.1 ka followed by a moderate return of Restionaceae pollen. This followed at the top of Pollen zone II (c. 9 ka), by a marked grass pollen increase.

Pollen zone III (8.5–4 ka) has lower resolution due to poor pollen preservation, but shows more grass and Asteraceae, including *Stoebe* type (probably including *Elytropappus*) up to about 6.5 ka when succulents like Aizoaceae and *Crassula*-type become prominent. Pollen zone IV (4–3 ka) at c. 3.8 ka shows prominent grasses, Asteraceae and eventually Restionaceae pollen and in a relatively short section up to c. 3.3 ka, although there is considerable variation in pollen composition. At c. 3.5–3.4 ka, types like *Morella* peak while others e.g., *Euclea* and

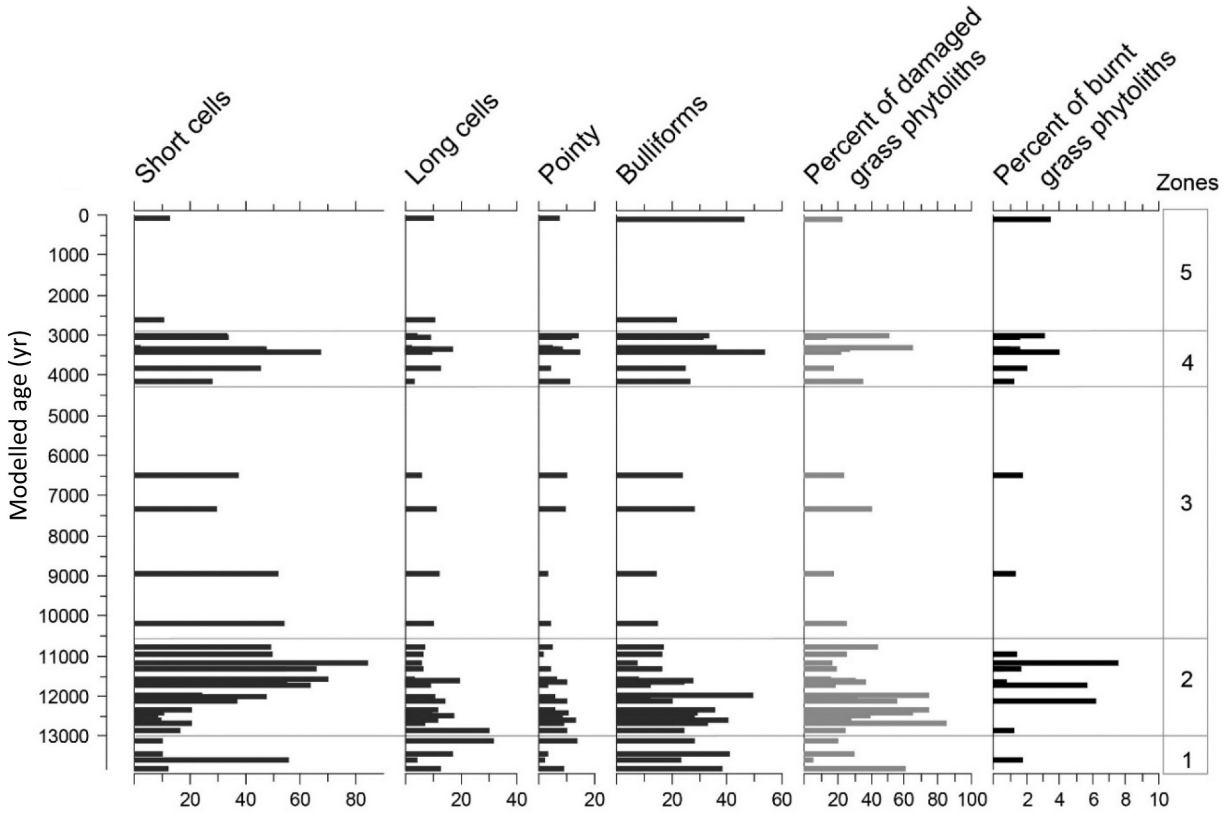

Fig. 6. Poaceae phytoliths and percent of burnt grass phytoliths.

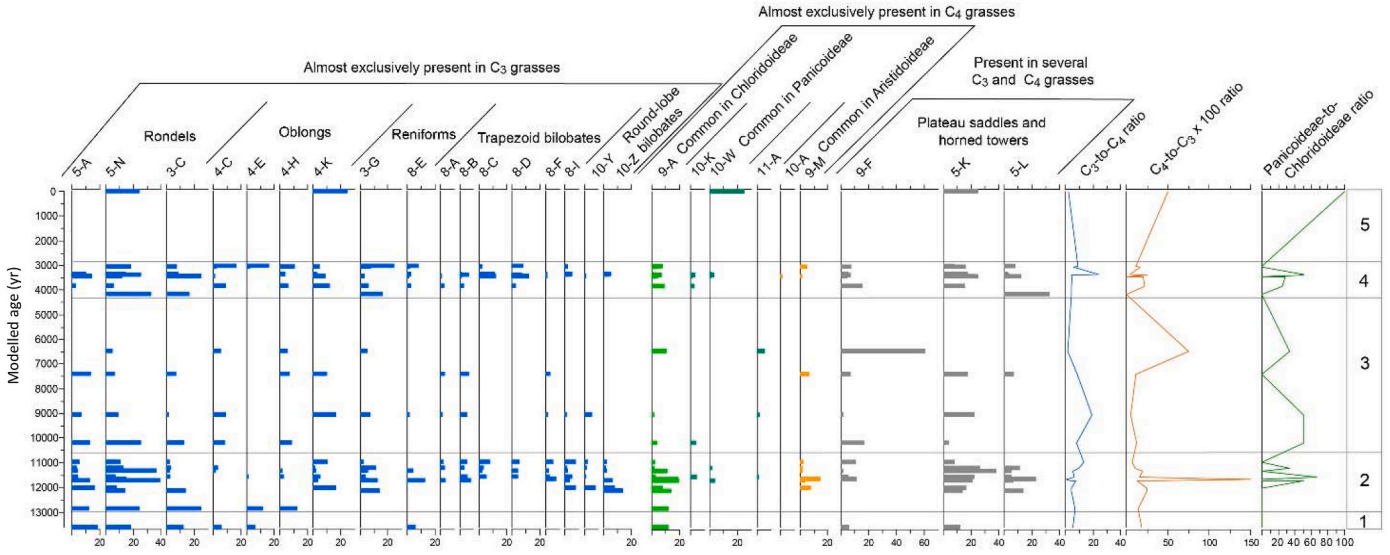

Fig. 7. Grass silica short cells (GSSC) and ratios.

Stoebe type, decline. The top section (Pollen zone V, 3 ka to the present) representing brown sands, is poorly covered as result of insufficient pollen preservation, but the available level at c. 2.6 ka is similar to the modern spectrum (Fig. 9).

5. Discussion

Transport of material from the higher ground probably influenced the different proxies. For instance, where karroid, succulent or grassy elements in the deposits occur, they probably reflect changing conditions in the source area within the uplands to the south, which is now under fynbos. This, via the presence of C_4 or CAM plants, may account for the varying composition of accompanying organic matter, phytoliths and pollen, and other inclusions from the surrounding slopes. Changes in rainfall seasonality, stream energy, etc., would also affect this. Mixed with the transported material are potentially the remains of local elements at the study site typical of the drainage course.

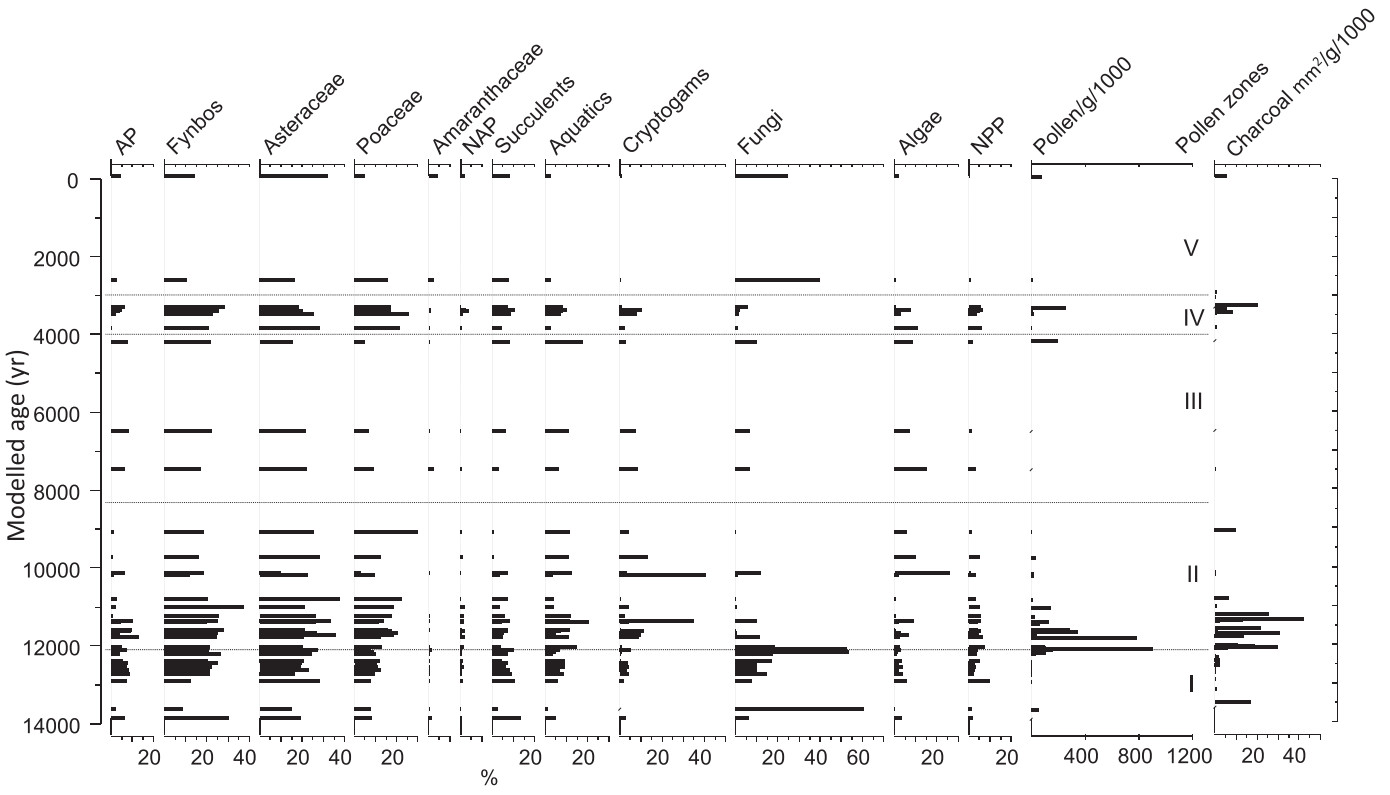

Fig. 8. Summary diagram of percentages of all palynomorph types. AP = arboreal pollen, NAP = other non-arboreal pollen, NPP = non-pollen palynomorphs. The columns on the right show pollen and microscopic charcoal concentrations (size classes in Fig. S4) and pollen zones (for creation of zones, see Fig. 9).

5.1. Geochemistry interpretation

The highly variable TOC content of the sediments largely reflects the varied depositional environment, with high TOC associated with fine grain sedimentary units, most likely overbank fines, waning limbs of flood events or palaeo-landsurfaces, and low TOC associated with flood deposits of coarse-grained sands and gravels. The former are particularly associated with the phase of relatively fast valley fill aggradation ~14–10 ka. The largely invariant TOC/TN ratios of 15–25 are typical of the measured range of Fynbos and Succulent Karoo Biome soils (Carr et al., 2013) (Fig. 4B), consistent with a largely terrestrial organic matter sediment source throughout the sequence. The lowest values of $\delta^{13}C_{TOC}$ are consistent with contributions from C_3 vegetation (global mean C_3 $\delta^{13}C$ -26‰; O'Leary, 1988; Diefendorf et al., 2010) (Fig. 4C, darker shading), and such values are characteristic of fynbos vegetation (Vogel et al., 1978; Carr et al., 2016). The higher $\delta^{13}C_{TOC}$ values (>−22‰) imply some contribution from non-C_3 vegetation, potentially including C_4 grasses ($\delta^{13}C$ typically −10 to −14‰; O'Leary, 1988) or CAM plants ($\delta^{13}C$ highly variable but high as −12‰; Rundel et al., 1999). Soils (Fig. 4C, lighter shading) in the Succulent Karoo biome, to which CAM plants may variably contribute organic matter, typically have $\delta^{13}C_{TOC}$ values of −22 to −23‰ (Carr et al., 2021). Soils in the Nama Karoo, for which C_4 grasses may contribute organic matter typically have $\delta^{13}C_{TOC}$ ranging between −22 and − 14‰, depending on grass cover/summer rainfall amount (Bond et al., 1994).

For the KMR record overall there is no correlation between $\delta^{13}C_{TOC}$ and grass pollen (Fig. 11A), but both C_3 and C_4 grasses were present based on the phytolith evidence (e.g., at c. 9 ka; Fig. 7, Fig. 12), and the latter parts of the record (e.g. 6–3 ka) show some potential correlation with grass pollen abundance, if not the phytolith-derived C_3/C_4 ratio. Other correlations between the isotope and pollen data are identified. The sum of the succulent pollen types (Fig. 11 B) correlates with $\delta^{13}C_{TOC}$ ($r = 0.37$ $p = 0.04$ for the whole record and more strongly (0.43, p = 0.04) for the section 14–9 ka (Fig. 11C, S6B/&b). Thus, one interpretation of the isotope data is that a varying proportion of CAM plants (succulents) contributed to the soil organic matter of the KMR catchment (Fig. 11B). As CAM physiology is essentially an adaptation to drought, this would imply that during periods of greater aridity there were greater inputs of CAM-plant derived organic matter from the catchment soils.

However, considering the $\delta^{13}C_{TOC}$ data in relation to the local pollen-fungal elements PCA axis 1 we also observe a correlation between these elements and $\delta^{13}C_{TOC}$ (Fig. 11C) (see Supplementary Material 1, Fig. S6B/7B). This reflects a positive (negative) correlation between $\delta^{13}C_{TOC}$ and fungal spores (local vegetation elements). The overall correlation with axis 1 is $r = 0.50$ ($p = 0.006$), with the correlation stronger for samples older than 10 ka ($r = 0.61$; $p = 0.004$) (Fig. 11C and D). The implied decreasing $\delta^{13}C_{TOC}$ in association with increased local/riparian/aquatic pollen inputs could therefore also reflect a shift in the sources of the organic matter input to the sediments; i.e. from a wider catchment contribution that includes CAM and soil fungi inputs to a dominantly local C_3 riparian / wetland vegetation input, which colonised the land-surface in the channel as it stabilised (also accounting for the accompanying increased TOC).

5.2. Vegetation conditions and trends

Here we summarize all proxies according to arbitrary time zones as phytolith and palynological zonations (Figs. 6–8 and Figs. 8–10) correspond broadly, but are not identical.

In 14–10.5 ka (8.9–4.5 m), predominantly organic-rich, layers of sand show high but steadily declining $\delta^{13}C_{TOC}$ values (except for a spike a spike within YD times at c. 12.2 ka (Fig. 4C), associated with increasing TOC. The proportions of Poaceae phytoliths, of which the majority are C_3 grasses, increase during this phase. The phytolith data provide further clues for the vegetation reconstruction ancillary to the pollen data, particularly for the graminoids. In the phytolith assemblage of 13.7–12.9 ka, the high incidence of non-graminoids (woody and

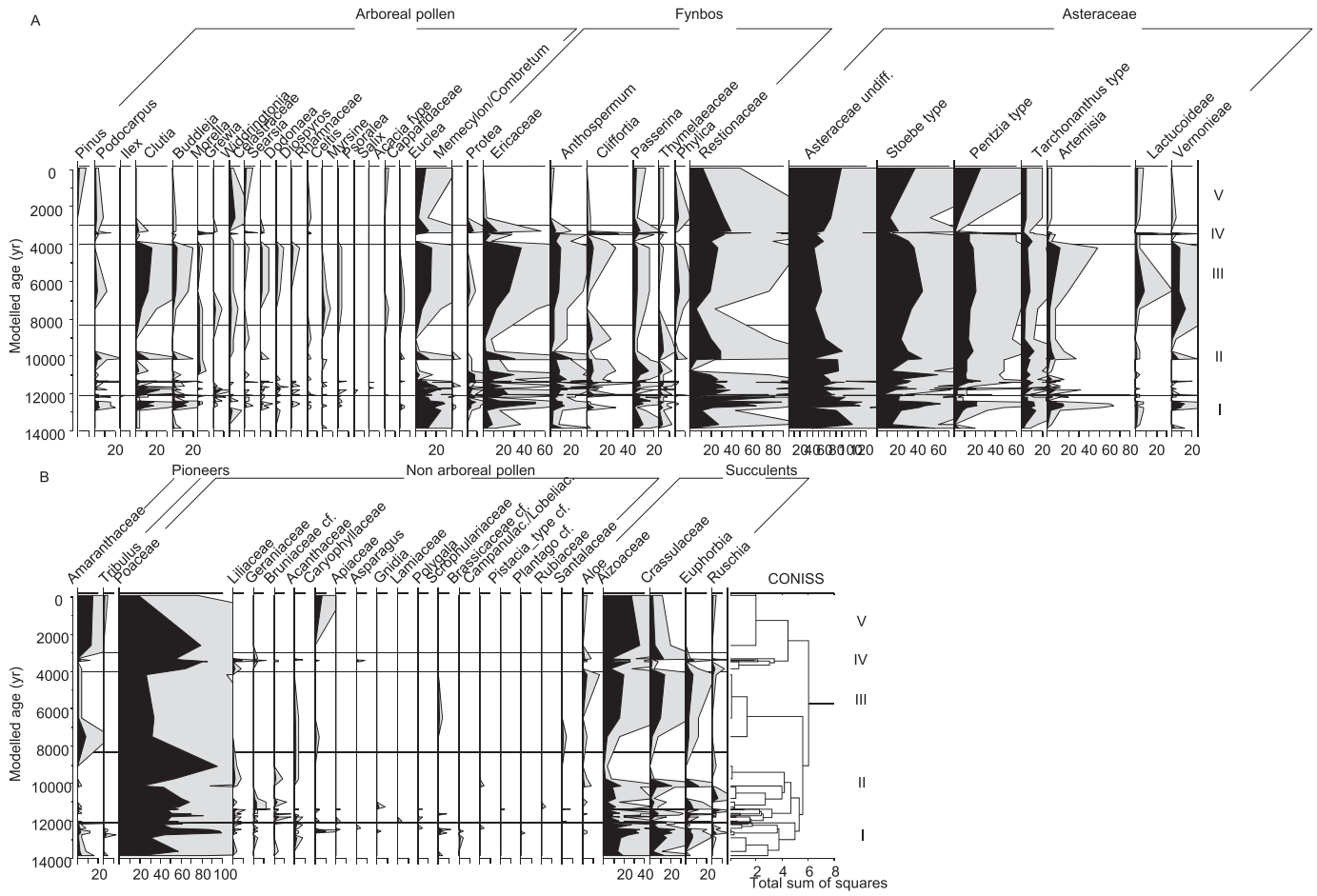

Fig. 9. A. Arboreal, fynbos and Asteraceae pollen. B pioneer, other non-arboreal and succulent pollen. Zones on the right in B are determined by the CONISS cluster diagram based on taxa represented in both A and B.

shrubby vegetation), abundant Restionaceae and relatively low proportions of Poaceae imply a dominance of fynbos vegetation (Cordova, 2013; Cordova and Avery, 2017). Distinctively, the burnt grass phytoliths count is lower. However, despite the limited Poaceae, there is an important incidence of C_3 grasses, suggesting some winter season rains. The relative importance of Chloridoideae suggests either occasional dryness or diminished summer rain.

The higher incidence of Poaceae over Restionaceae and the lower proportions of non-graminoids c. 12.9–10.6 ka suggest a grassier environment, still within a matrix of Ericaceous fynbos. This could be a type of grassy fynbos like the ones found farther east (cf. Rebelo et al., 2006) or the amplification of the renosterveld (*Stoebe* type), which normally has more grasses (Cordova, 2013; Cordova and Avery, 2017). However, given the incidence of Panicoideae, it is possible that increased summer rain prompted more lightning-initiated fires, as it currently occurs in areas of fynbos farther east, thus promoting the spread of grasses and the decline of Ericaceae and Thymeleaceae. The pollen data further suggest grassy karroid vegetation, which probably included *Elyropappus* (*Stoebe* type), with some fynbos elements, especially Restionaceae, and decreasing succulent abundance. The latter may explain the high but declining $\delta^{13}C_{TOC}$ through this period, although this reduction in $\delta^{13}C_{TOC}$ may also reflect the aforementioned increased organic matter inputs from local aquatic (C_3) vegetation, which also peak ~11 ka. Both the burned phytoliths and the charcoal suggest increased burning ~12 ka within the YD phase.

The period 10.5–7 ka (4.5–3.3 m) is associated with a much-reduced sample resolution and some gravel inclusions that probably experienced erosion. It consists otherwise of grey to black organic sands, rich in TOC up to 10 ka, but declining from c. 9 ka, with relatively low $\delta^{13}C_{TOC}$ (likely C_3 vegetation derived) (Figs. 4 and 13). At around 10 ka, there is a brief peak of montane woodland pollen, e.g., *Podocarpus*, *Clutia*, *Buddleja* and *Euclea* together with fynbos (Fig. 9A). Next during this phase, high percentages of grass phytoliths and grass pollen occur at c. 9 ka. Judging from the isotope and phytolith composition the parent plants were predominantly C_3 grasses, but C_4 grasses were also present (Figs. 7, 12), which occurred together with Restionaceae, undifferentiated Asteraceae and *Stoebe* type (probably, also including *Elytropappus*) (Figs.9A).

The sandy section, 7 ka–4.1 ka (3.3–2.9 m), associated with relatively low TOC contents (Fig. 4A) accumulated relatively slowly and preserves few pollen and phytoliths, possibly due to exposure and drying. It shows relatively low $\delta^{13}C_{TOC}$ values c. 7–6.5 ka (sequence minimum value of −25.6‰ at c. 4.2 ka) (Fig. 4C). The absolute values in both periods suggest dominantly C_3 vegetation inputs, although there is marginally higher $\delta^{13}C_{TOC}$ at 7–6.5 ka, coeval with a single phytolith level (6.5 ka) (Fig. 7) that indicates an increased C_4 grass component. Around 6.5 ka we observe an increase in succulent pollen together with other mountain slope vegetation like Ericaceae, *Euclea* and *Clutia*. The proportions of phytolith assemblages and GSSC distribution prior to c. 6.0 ka provide limited information, although it is possible that rainfall was equally spread during summer and winter. After 6.0 ka there is a reduction in woody/shrubby vegetation and an apparent increase in Chloridoideae, which may reflect dry conditions similar to the Succulent Karoo, where Chloridoideae grasses tend to dominate (Cordova and Scott, 2010; Cordova, 2013).

The section, 4.1–2.6 ka (1.9–0.6 m), starts with an iron stained

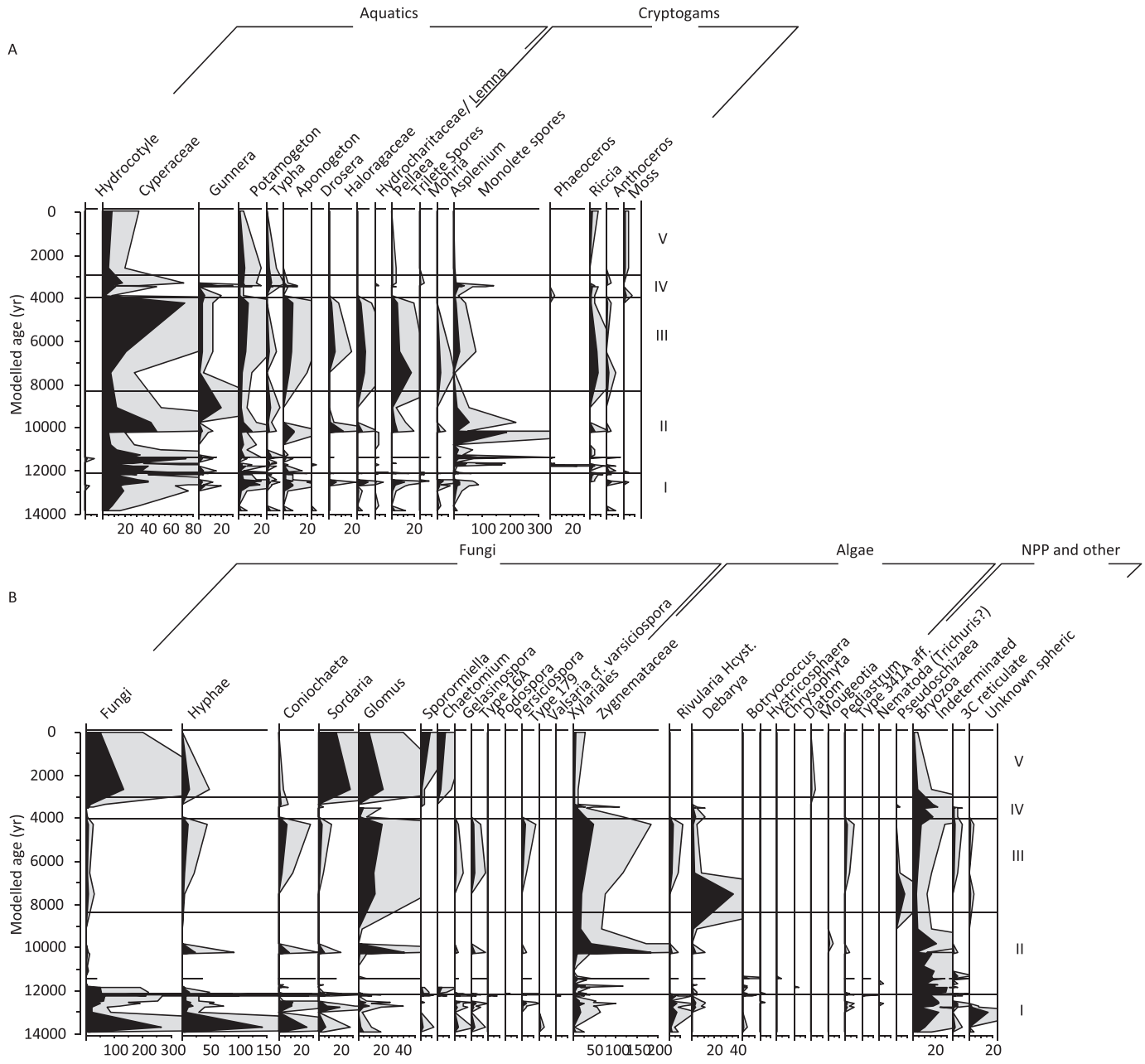

Fig. 10. Aquatic pollen, cryptogam spores and NPP's. Pollen zones on the right are based on the regional taxa in Fig. 9.

orange sand covered by grey sands. The TOC content varies but is generally low except for some darker grey horizons and $\delta^{13}C_{TOC}$ increases to values more akin to those of the late Pleistocene (−23.5‰). The phytolith assemblages suggest the expansion of fynbos, but unlike the period c. 12.9–10.6 ka, this fynbos has a higher incidence of grasses, with evidence for frequent burning (Fig. 6). Grass phytoliths are mainly of the C_3 type with little C_4 representation, but a variable to strong succulent presence in the pollen data may account for the $\delta^{13}C_{TOC}$ trend. Typical woody slope elements, Asteraceae and fynbos, including Restionaceae are present, especially at c. 3.4 ka. It is possible that winter rains were dominant, but at times summer rains must have occurred, perhaps even more than today.

The brownish upper sands, 2.6–0 ka (0.6 m–0 m), do not preserve pollen and phytoliths. However, the modern surface sample shows a strong presence of Poaceae phytolith morphotypes with some C_4 grass representation, Asteraceae and succulent pollen.

5.3. General synthesis of environmental changes of the KMR sequence

The opposing dynamics between Poaceae and Asteraceae and other fynbos and succulent taxa observed in the KMR sequence are not reflected in the modern pollen transect (Supplementary Material 1, Fig. S5). This is, however, not unexpected as in the modern transect the higher grass proportions towards the karroid vegetation to the north, represent mostly C_4 grass (cf. Cordova and Avery, 2017, their Figs. 5a and 8), while we have phytolith evidence that the grass peaks in the fossil sequence largely represent C_3 grass. The question then arises as to what conditions the combination of C_3 grasses and Asteraceae observed at 9 ka in the KMR would imply (Fig. 9, Fig. S6A and S7A). If it represented a cool, relatively dry environment with winter growth, this would find support in the (low) $\delta^{13}C_{TOC}$ values. After 8 ka some C_4 grasses occur, but with only slightly increased isotope values. The $\delta^{13}C_{TOC}$ decreases before 4 ka, at a time when fynbos including Ericaceae, Restionaceae and *Stoebe* type, probably including *Elytropappus* (renosterbos), is

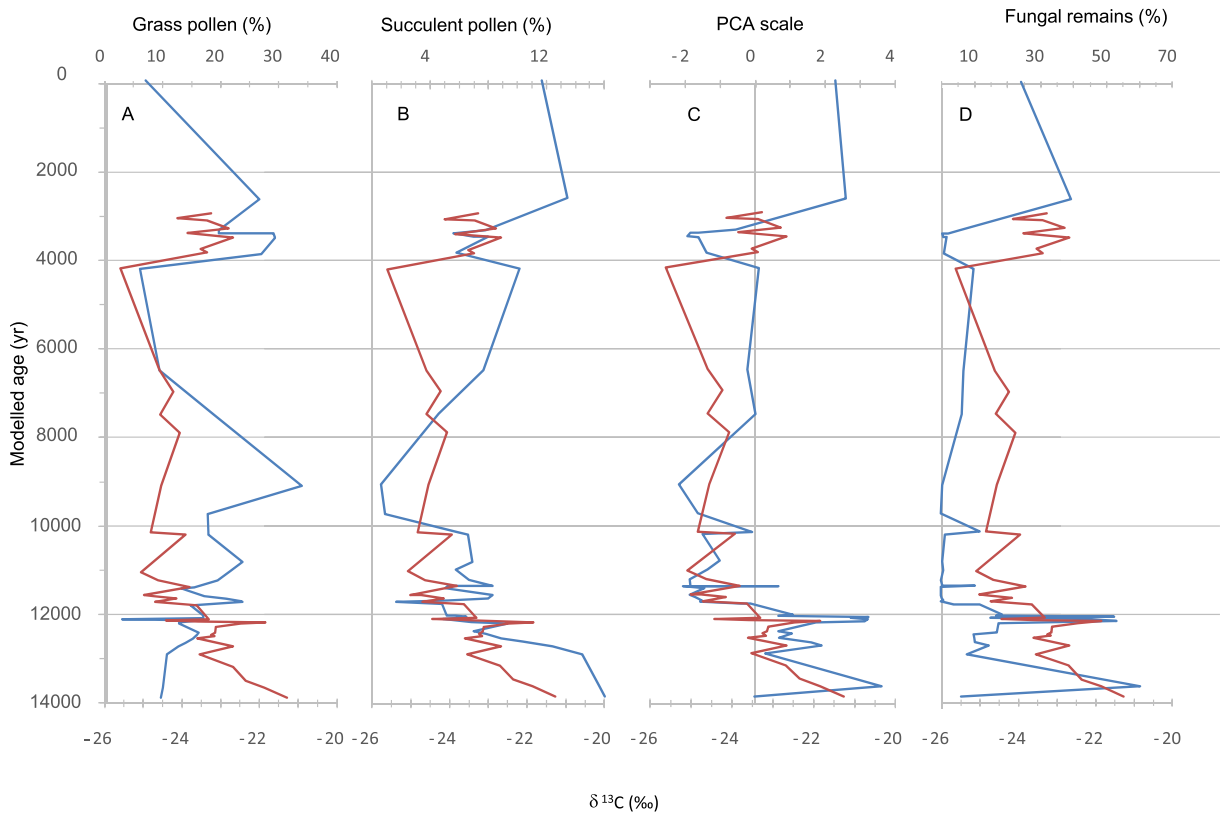

Fig. 11. A. Loess smoothed grass (blue) and $\delta^{13}C_{TOC}$ (red). B. Slightly Loess smoothed summed succulents (blue) and $\delta^{13}C_{TOC}$ (red). C. Local pollen & spore PCA axis 1 (blue) vs. $\delta^{13}C_{TOC}$ (red). D. Fungi (blue) % vs. $\delta^{13}C_{TOC}$ (red). (For interpretation of the references to colour in this figure legend, the reader is referred to the web version of this article.)

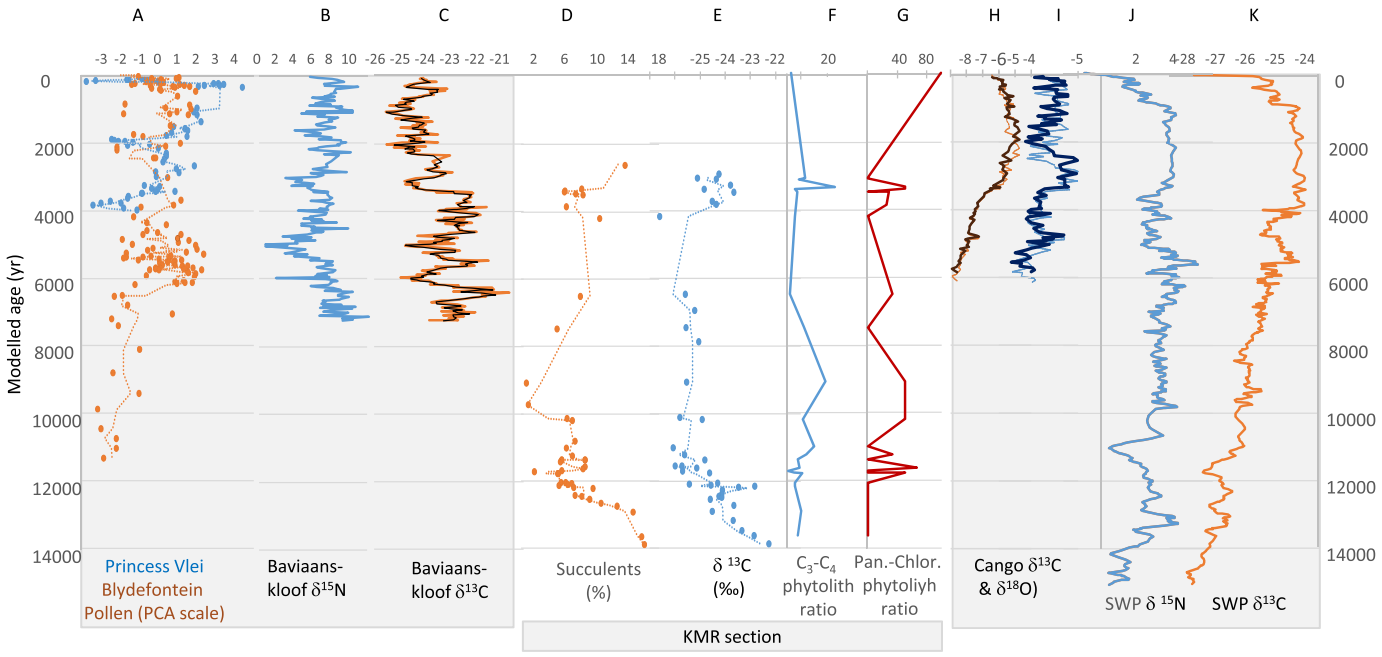

Fig. 12. The KMR section with various proxies from the Western and Eastern Cape Provinces (numbers in brackets refer to positions in Fig. 1A.). A. Pollen PCs Blydefontein (7) (brown) (Scott et al., 2012, chronology adjusted) and Princess Vlei (14) (blue) (Neumann et al., 2011; Cordova et al., 2019), B. Baviaanskloof (8), $\delta^{15}N$ ‰, C. $\delta^{13}C$ ‰ (Chase et al., 2020), D. KMR, Succulent pollen %, E. KMR $\delta^{13}C_{TOC}$ ‰, F. KMR C_3/C_4 phytolith ratio, G. KMR Panicoideae/Chloridoideae phytolith ratio (this study), H. Cango Caves (9): $\delta^{13}C$ ‰, I. $\delta^{18}O$‰ (solid lines Talma and Vogel, 1992, faded lines Chase et al., 2013 chronology), J. Seweweekspoort (10) J. $\delta^{15}N$‰, K. $\delta^{13}C$ (‰) (Chase et al., 2013, 2018). (For interpretation of the references to colour in this figure legend, the reader is referred to the web version of this article.)

observed to increase in the pollen spectra. This vegetation suggests relatively moist conditions.

Alternations of aquatic pollen types, cryptogam spores, fungal spores and algae can be related to interaction between flooding events, stream energy, stream transport, fungal decay and selective preservation. There are marked trends in the occurrence of fungal remains through the sequence. For the period 14–11 ka there are elevated, albeit declining fungal elements (Fig. 11D) and initially reduced local wetland, cryptogamic and algal elements, which become increasingly abundant towards 11 ka. Indeed, during this phase there is a correlation between fungal elements and the $\delta^{13}C_{TOC}$, under otherwise cool, dry and relatively stable conditions, while according to the phytoliths, a transition to more C_3 vegetation took place and fungal remains declined. The process was gradual except for a brief reversal during YD times. This is also a period associated with steady accumulation of the sediment sequence (i.e. aggradation of the fluvial system), possibly transporting soil fungi from the surrounding slopes, although it is not possible to determine how much was transported or locally produced. Fungal remains in the deposits subsequently decline in favour of active local plant and algal growth up to around 4–3 ka (Fig. 11 D) (PC 1, Fig. 11 C, see also Fig. S6B/S7B in Supplementary Material 1) where there is a shift in $\delta^{13}C_{TOC}$ that coincides with increased succulent pollen, potentially implying increased CAM or C_4 vegetation contributions. The return of fungal remains is, however, delayed until 2.6 ka when drier conditions set in and there is a more prominent appearance of succulent Aizoaceae type pollen (Fig. 11 B). The increase in fungal remains can either be attributed to the more stable soil formation processes at the site itself or to transport of soil material from the surrounding slopes, or both.

5.4. Regional comparisons

The KMR sequence provides several lines of evidence potentially indicative of changes in rainfall amount and seasonality. The findings can be placed in a wider context to reconstruct a regional history through comparison with other proxy sequences (Fig. 12). Notably, the nearest palaeoenvironmental record is the Baviaanskloof Rock hyrax midden record ~50 km to east. This provides evidence for vegetation ($\delta^{13}C$) and climatic ($\delta^{15}N$) changes over the last 7 ka (Chase et al., 2020) (Fig. 12B &C). ~80 km to the west of KMR, the Cango Cave stalagmite record provides temperature ($\delta^{18}O$) and vegetation ($\delta^{13}C$) proxies spanning the last 6 ka (Talma and Vogel, 1992) (Fig. 12A). Cango Caves lie close to the Boomplaas Cave archaeological site, for which a recent reconstruction of rainfall seasonality and rainfall amount has been presented using micromammal evidence (Faith et al., 2018), while 150 km to the west, the longer hyrax dung sequence from Seweweekspoort (Fig. 12J, K) (Chase et al., 2013, 2018) provides both isotope and pollen evidence from marine isotope stage 2 to the present.

In KMR, the dominantly present C_3 grass phytoliths (with C_4 present, but never dominant), the high incidence of non-graminoids (woody and shrubby vegetation) and the abundant Restionaceae observed 14–10.5 ka are not inconsistent with recent reconstructions of a relatively humid, mixed summer-winter rainfall environment for the latest Pleistocene (i.e. last glacial-interglacial transition) (Chase et al., 2018; Faith et al., 2018). The trend in $\delta^{13}C_{TOC}$ and succulent pollen at KMR during this phase (both peaking at 14 ka and potentially implying some aridity), presents potential evidence for variability around this scenario (indeed, it is opposed to the overall increasing trend in $\delta^{13}C$ seen it the SWP record (Fig. 12) (Chase et al., 2018). However, the Seweweekspoort $\delta^{15}N$ record (Chase et al., 2018) indicates short-term variability in water availability within the 15–10 ka period, with a trend from relatively arid to relatively wetter conditions ~13.3–11 ka (Fig. 12) that is perhaps consistent with observations at KMR, including the reduction in succulent pollen observed during this period. Based on the Boomplaas micromammal record, Faith et al. (2018) presented a reconstruction for the Pleistocene-Holocene transition that indicated increasing winter rainfall contributions from ~13–10 ka, associated with a trend towards relatively arid conditions. Consistent with this, at KMR the phytolith data show a steady reduction in the C_4/C_3 ratio to a minimum at ~10 ka. Additionally, by 9 ka, relatively more C_3 grasses developed (Fig. 7, 12F) in a grassier, more frequently burned environment with a higher incidence of Poaceae over Restionaceae and lower proportions of non-graminoids c. 12.9–10.6 ka and at 9 ka. The precession cycle (Berger and Loutre, 1991) would have promoted winter rainfall at around 9 ka (Street-Perrott and Perrott, 1993; Partridge et al., 1997).

Given the low sampling resolution for the early to mid-Holocene, detailed comparisons are challenging, especially c. 4–7 ka when there seems to be much variability in several records, notably the sharp c. 5 ka negative (increased humidity) deviation in $\delta^{15}N$ at Baviaanskloof (Chase et al., 2020). By 6.5 ka precessional forcing in this all-year seasonality zone would probably favoured slightly more summer rains, but moderately dry conditions with succulents and Asteraceae persisted, with some C_4 grass (more apparent from phytoliths than isotope values).

The resolution at KMR is too poor to draw conclusions as to the effects of the maximum sea ice extent in the South Atlantic at ~4.3 ka (Nielsen et al., 2004). However, the period 4–2 ka offers an opportunity for comparison with several records. Here KMR record shows a $\delta^{13}C_{TOC}$ minimum (−25.6‰) at or prior to ~4.2 ka and then stabilises at ~−23‰ from 3.7–3.1 ka. This transition is associated with relatively grassy fynbos vegetation, increased succulent pollen and increased evidence of burning. The Cango Cave speleothem (Talma and Vogel, 1992) exhibits an increase in $\delta^{13}C$ starting at 3 ka and peaking by c. 2 ka (Fig. 12I). However, Chase et al. (2013) suggest a revised chronology that places this peak at c. 3 ka. The SWP midden, which also exhibits its highest grass pollen concentrations at this time, has high $\delta^{13}C$ values between 3 and 1 ka (Fig. 12K) (Chase et al., 2018). These observations are consistent with the increased abundance of grass pollen and phytoliths at KMR c. 3 ka, where interestingly (for interpretation of $\delta^{13}C$ trends) the phytolith data suggest this was largely C_3 grass with lower amounts of C_4 types (Fig. 12D-G). At Cango the associated $\delta^{18}O$ temperature record indicates a relatively sharp 1 °C increase at about <2 ka (Talma and Vogel, 1992; Fig. 12H) but Chase et al. (2013) suggest that this occurred at about 3 ka. At the same time the Baviaanskloof midden also shows a marked change in $\delta^{13}C$ and $\delta^{15}N$, although the direction of the former proxy (a shift to lower $\delta^{13}C$) is opposite to that observed at SWP and Cango Caves (i.e. it is reduced, implying more C_3 vegetation consumption by the hyraxes, perhaps dependent on their dietary preferences for available plant species). Overall however, the year-round rainfall zone exhibits consistent evidence for a marked climatic/ecological transition at this time, presumably in response to increased temperatures (Talma and Vogel, 1992; Chase et al., 2013). Whether such increased temperature was associated with reduced winter rainfall/increased summer rainfall (see Chase et al., 2017, 2018) is less clear given the apparently limited response in the KMR phytolith data and the contrasting $\delta^{13}C$ trajectories in the hyrax midden records. Indeed, the increase in succulent pollen at KMR is consistent with reduced moisture availability (i.e. aridity) associated with such a temperature increase, as might be the reduced palatability/availability (for hyraxes) of (C_4) grasses (Chase et al., 2020).Considering regional climatic drivers, the KMR sequence can be viewed in terms of the hypothesis of Chase and Quick (2018), which emphasises the role of the warm Agulhas current in driving climatic variability in the southern coastal region, in direct contrast to drivers and trends in the relatively nearby southern interior areas. The Seweweekspoort record c. 80 km from the coast (Chase et al., 2017; Chase and Quick, 2018) provided evidence to support this hypothesis, while the Baviaanskloof record, if differing in detail, provides some further support for this coastal-interior dichotomy. In this sense comparisons between these interior sites and KMR broadly provide support this model (in general if not perhaps in terms of details at smaller temporal scales).

Deeper inland from KMR, ~ 330 km to the northeast, is the Blydefontein site in the summer rain region of the Nama Karoo Biome (Mucina and Rutherford, 2006). Here the Holocene pollen record provides

evidence of moisture availability based on grass cover versus karroid shrub cover (Scott et al., 2005, 2012; Scott et al., 2020). After a humid spell between 6 and 4.5 ka it suggests relative dryness, probably a decline in summer rain, occurred just before 4 ka at the time when at KMR succulents, renosterbos (*Stoebe* type), other Asteraceae and Ericaceae were prominent and grasses were reduced. The change to wetter conditions that follows, suggest a regional climatic coherence between Blydefontein and KMR in terms of moisture availability for the time between c. 4.2 ka and 3 ka. Both seem to follow the interior pattern that is also inferred at Cango Caves and Seweweekspoort (Chase et al., 2013, 2020; Chase and Quick, 2018). This is not the case in the coastal area at Eilandvlei (Quick et al., 2018) and Still Bay (Quick et al., 2015), where a decline in afro-temperate forest is evident just before 4 ka, or at Princess Vlei further to the west where pollen suggest relatively dry conditions (Fig. 12) at this time (Neumann et al., 2011; Cordova et al., 2019). The pattern of climate development at KMR sequence therefore seems to conform to that in the interior rather than the coastal pattern, as proposed by Chase and Quick (2018), even if it is only about 40 km from the coast.

6. Conclusions

The Holocene KMR section provides the first multi-proxy study of palaeoenvironments as derived from an alluvial sequence in the relatively dry all-year rainfall zone in the Western and Eastern Cape border area. It demonstrates how the different proxies complement each other and contribute to our understanding of changing conditions in a complex depositional system. The sequence of deposits starts shortly before the Northern Hemisphere's Younger Dryas event. At this time we observe relatively fast accumulation of deposits under dry conditions. Together the lithology, isotope, phytolith and pollen data suggest a shift towards alternating phases of humid and dry events with higher stream energy, slower accumulation and subtly changing seasonality during the early and middle Holocene, as far as can be ascertained from the relatively low sample resolution. By c. 4 ka a relatively humid phase started after which pollen and phytolith preservation in the upper layers became poor, presumably due to drier conditions.

In terms of regional forcing, the results suggest that the climatic development at KMR during the Holocene, a location only c. 40 km from the coast, despite minor short-term deviations, conforms more to patterns identified in the interior Karoo region than to those observed in peri-coastal sites. To further investigate the geographic scope of coastal Agulhas Current climate forcing, a similar set of deposits of the same age has been located further to the south (Louterwater, in the Langkloof, c. 30 km from the coast), which will allow us to test this hypothesis in further studies.

Declaration of Competing Interest

None.

Acknowledgements

We thank Peter Holmes, who accompanied us to the studied site and coined the term KMR based on the Kamanassie River. Martin Wessels and Maitland Seaman assisted with fieldwork and photography. Andri van Aardt is thanked for laboratory and travel arrangements. LS was supported by the National Research Foundation (South Africa) (NRF Grant 85903). SM was supported by the NRF Competitive Programme for Rated Researchers (South Africa) (Grant 118538) and a travel grant from the Ministry of Economy and Competitiveness (Spain) and JO and JSC by Project CGL-PID2019-1049449GB-I00 (FEDER/Ministry of Science and Innovation, Spain). ASC's contribution was supported by the Leverhulme Trust (Grant F/00 212/AF).

Appendix A. Supplementary data

Supplementary data to this article can be found online at https://doi.org/10.1016/j.palaeo.2021.110331.

References

Carr, A.S., Chase, B.M., Boom, A., Meadows, M.E., 2021. Soil and Foliar Stable Carbon and Nitrogen Isotope Compositions in the Fynbos and Succulent Karoo Biomes (In prep).
Berger, A., Loutre, M.F., 1991. Insolation values for the climate of the last 10 million years. Quat. Sci. Rev. 10, 297–317.
Blaauw, M., Christen, J.A., 2011. Flexible paleoclimate age-depth models using an autoregressive gamma process. Bayesian Anal. 6, 457–474.
Bond, W.J., Stock, W.D., Hoffman, M.T., 1994. Has the Karoo spread? A test for desertification using carbon isotopes from soils. S. Afr. J. Sci. 90, 391–397.
Bousman, C.B., Partridge, T.C., Scott, L., Metcalfe, S.E., Vogel, J.C., Seaman, M., Brink, J. S., 1988. Palaeoenvironmental implications of Late Pleistocene and Holocene valley fills in Blydefontein basin, Noupoort, C.P., South Africa. Palaeoecol. Africa 19, 43–67.
Carr, A.S., Boom, A., Chase, B.M., Meadows, M.E., Roberts, Z.E., Britton, M.N., Cumming, A.M.J., 2013. Biome-scale characterisation and differentiation of semi-arid and arid zone soil organic matter compositions using pyrolysis-GC/MS analysis. Geoderma 200-201, 189–201.
Carr, A.S., Chase, B.M., Boom, A., Medina-Sanchez, J., 2016. Stable isotope analyses of rock hyrax faecal pellets, hyraceum and associated vegetation in southern Africa: implications for dietary ecology and palaeoenvironmental reconstructions. J. Arid Environ. 134, 33–48.
Chase, B.M., Meadows, M.E., 2007. Late Quaternary dynamics of southern Africa's winter rainfall zone. Earth Sci. Rev. 84, 103–138.
Chase, B.M., Quick, L., 2018. Influence of Agulhas forcing of Holocene climate change in South Africa's southern Cape. Quat. Res. 2018, 1–7.
Chase, B.M., Boom, A., Carr, A.S., Meadows, M.E., Reimer, P.J., 2013. Holocene climate change in southernmost South Africa: rock hyrax middens record shifts in the southern westerlies. Quat. Sci. Rev. 82, 199–205.
Chase, B.M., Lim, S., Chevalier, M., Boom, A., Carr, A.S., Meadows, M.E., Reimer, P.J., 2015. Influence of tropical easterlies in southern Africa's winter rainfall zone during the Holocene. Quat. Sci. Rev. 107, 138–148.
Chase, B.M., Chevalier, M., Boom, A., Carr, A.S., 2017. The dynamic relationship between temperate and tropical circulation systems across South Africa since the Last Glacial Maximum. Quat. Sci. Rev. 174, 54–62.
Chase, B.M., Faith, J.T., Mackay, A., Chevalier, M., Carr, A.S., Boom, A., Lim, S., Reimer, P.J., 2018. Climatic controls on Later Stone Age human adaptation in Africa's southern Cape. J. Hum. Evol. 114, 36–45.
Chase, B.M., Boom, A., Carr, A.S., Quick, L.J., Riemer, P.J., 2020. High-resolution record of Holocene climate change dynamics from southern Africa's temperate-tropical boundary, Baviaanskloof, South Africa. Palaeogeogr. Palaeoclimatol. Palaeoecol. 539, 109518.
Chevalier, M., Chase, B.M., 2015. Southeast African records reveal a coherent shift from high- to low-latitude forcing mechanisms along the east African margin across last glacial-interglacial transition. Quat. Sci. Rev. 125, 117–130.
Cohen, T.J., Nanson, G.C., 2007. Mind the gap: an absence of valley-fill deposits identifying the Holocene hypsithermal period of enhanced flow regime in southeastern Australia. The Holocene 17 (3), 411–418.
Cordova, C.E., 2013. C_3 Poaceae and Restionaceae phytoliths as potential proxies for reconstructing winter rainfall in South Africa. Quat. Int. 287, 121–180.
Cordova, C., Avery, G., 2017. African savanna elephants and their vegetation associations in the Cape Region, South Africa: Opal phytoliths from dental calculus on prehistoric, historic and reserve elephants. Quat. Int. 443, 189–211.
Cordova, C.E., Scott, L., 2010. The potential of Poaceae, Cyperaceae, and Restionaceae phytoliths to reflect past environmental conditions in South Africa. Palaecol. Afr. 107–133.
Cordova, C.E., Kirsten, K.L., Scott, L., Meadows, M., Lücke, A., 2019. Multi-proxy evidence of late-Holocene paleoenvironmental change at Princessvlei, South Africa: the effects of fire, herbivores, and humans. Quat. Sci. Rev. 221, 105896.
Diefendorf, A.F., Mueller, K.E., Wing, S.L., Koch, P.L., Freeman, K.H., 2010. Global patterns in leaf ^{13}C discrimination and implications for studies of past and future climate. Proc. Natl. Acad. Sci. 107, 5738–5743.
Faegri, K., Iversen, J., 1989. Textbook of Pollen Analysis, 4th edition. JohnWiley and Sons, New York.
Faith, J.T., Chase, B.M., Avery, D.M., 2018. Late Quaternary micromammals and the precipitation history of the southern Cape, South Africa. Quat. Res. 1–13 https://doi.org/10.1017/qua.2018.105.
Fischer, H., Fundel, F., Ruth, U., Twarloh, B., Wegner, A., Udisti, R., Becagli, S., Castellano, E., Morganti, A., Severi, M., Wolff, E., Littot, G., Röthlisberger, R., Mulvaney, R., Hutterli, M.A., Kaufmann, P., Federer, U., Lambert, F., Bigler, M., Hansson, M., Jonsell, U., de Angelis, M., Boutron, C., Siggaard-Andersen, M.-L., Steffensen, J.P., Barbante, C., Gaspari, V., Gabrielli, P., Wagenbach, D., 2007. Reconstruction of millennial changes in dust emission, transport and regional sea ice coverage using the deep EPICA ice cores from the Atlantic and Indian Ocean sector of Antarctica. Earth Planet. Sci. Lett. 260, 340–354.
Grimm, E., 2011. TILIA Software, version 1.7. 16. Illinois State Museum, Research and Collection Center, Springfield, IL.

Hogg, A.G., Hua, Q., Blackwell, P.G., Buck, C.E., Guilderson, T.P., Heaton, T.J., Niu, M., Palmer, J., Reimer, P.J., Reimer, R., Turney, C.S.M., Zimmerman, S.R.H., 2013. ShCal13 Southern Hemisphere calibration, 0-50,000 cal yr BP. Radiocarbon 55 (4). https://doi.org/10.2458/azu_js_rc.55.16783.

Lim, S., Chase, B.M., Chevalier, M., Reimer, P.J., 2016. 50,000 years of vegetation and climate change in the southern Namib Desert, Pella, South Africa. Palaeogeogr. Palaeoclimatol. Palaeoecol. 451, 197–209.

Martin, A.R.H., 1968. Pollen analysis of Groenvlei lake sediments, Knysna (South Africa). Rev. Palaeobot. Palynol. 7, 107–144.

Mucina, L., Rutherford, M.C., 2006. The Vegetation of South Africa, Lesotho, and Swaziland, Strelitzia, 19. South African National Biodiversity Institute, Pretoria.

Munsterman, M., Kerstholt, S., 1996. Sodium polytungstate, a new non-toxic alternative to bromoform in heavy liquid separation. Rev. Palaeobot. Palynol. 91, 417–422.

Neumann, F.H., Scott, L., Bamford, M., 2011. Climate change and human disturbance of fynbos vegetation during the late Holocene at Princess Vlei, Western Cape, South Africa. The Holocene 21 (7), 1137–1150.

Nielsen, S.H.H., Koç, N., Crosta, X., 2004. Holocene climate in the Atlantic sector of the Southern Ocean: controlled by insolation or oceanic circulation? Geology 32, 317–320.

O'Leary, M.H., 1988. Carbon isotopes in photosynthesis. Bioscience 38, 328–336.

Partridge, T.C., Demenocal, P.B., Lorentz, S.A., Paiker, M.J., Vogel, J.C., 1997. Orbital forcing of climate over South Africa: a 200 000-year rainfall record from the Pretoria Saltpan. Quat. Sci. Rev. 16, 1–9.

Quick, L.J., Chase, B.M., Meadows, M.E., Scott, L., Reimer, P.J., 2011. A 19.5 kyr vegetation history from the Central Cederberg Mountains, South Africa: Palynological evidence from rock hyrax middens. Palaeogeogr. Palaeoclimatol. Palaeoecol. 309, 253–270.

Quick, L.J., Carr, A.S., Meadows, M.E., Boom, A., Bateman, M.D., Roberts, D.L., Reimer, P.J., Chase, B.M., 2015. A late Pleistocene-Holocene multi-proxy record of palaeoenvironmental change from still Bay, southern Cape coast, South Africa. J. Quat. Sci. 30 (8), 870–885.

Quick, L., Carr, A.S., Meadows, M.E., Boom, A., Bateman, M.D., Roberts, D.L., Reimers, P. J., Chase, B.M., 2016. A late PleistoceneeHolocene multi-proxy record of palaeoenvironmental change from Still Bay, southern Cape Coast, South Africa. J. Quat. Sci. 30, 870–885.

Quick, L.J., Chase, B.M., Wündsch, M., Kirsten, K.L., Chevalier, M., Mäusbacher, R., Meadows, M.E., Haberzettl, T., 2018. A high-resolution record of Holocene climate and vegetation dynamics from the southern Cape coast of South Africa: pollen and microcharcoal evidence from Eilandvlei. J. Quat. Sci. 33, 487–500.

Rebelo, A.G., Boucher, C., Helme, N., Mucina, L., Rutherford, M.C., 2006. Fynbos biome. In: Mucina, L., Rutherford, M.C. (Eds.), The Vegetation of South Africa, Lesotho, and Swaziland, Strelitzia 19. South African National Biodiversity Institute, Pretoria, pp. 53–219.

Rundel, P.W., Esler, K.J., Cowling, R.M., 1999. Ecological and phylogenetic patterns of carbon isotope discrimination in the winter-rainfall flora of the Richtersveld, South Africa. Plant Ecol. 142, 133–148.

Scholtz, A., 1986. Palynological and Palaeobotanical Studies in the Southern Cape. University of Stellenbosch, Stellenbosch.

Scott, L., 1996. Palynology of hyrax middens: 2000 years of palaeo-environmental history in Namibia. Quat. Int. 33, 73–79.

Scott, L., Vogel, J.C., 2000. Evidence for environmental conditions during the last 20,000 years in Southern Africa from ^{13}C in fossil hyrax dung. Glob. Planet. Chang. 26 (1–3), 207–215.

Scott, L., Woodborne, S., 2007a. Pollen analysis and dating of late quaternary faecal deposits (hyraceum) in the Cederberg, Western Cape, South Africa. Rev. Palaeobot. Palynol. 144, 123–134.

Scott, L., Woodborne, S., 2007b. Vegetation history inferred from pollen in late Quaternary faecal deposits (hyraceum) in the Cape winter-rain region and its bearing on past climates in South Africa. Quat. Sci. Rev. 26, 941–953.

Scott, L., Bousman, C.B., Nyakale, M., 2005. Holocene pollen from swamp, cave and hyrax dung deposits at Blydefontein (Kikvorsberge), Karoo, South Africa. Quat. Int. 129, 49–59.

Scott, L., Neumann, F.H., Brook, G.A., Bousman, C.B., Norström, E., Metwally, A.A., 2012. Terrestrial fossil Pollen evidence of climate Change during the last 26 Thousand Years in Southern Africa. Quat. Sci. Rev. 32, 100–118.

Scott, L., Sobol, M., Neumann, F.H., Gil Romera, G., Fernández-Jalvo, Y., Bousman, C.B., Horwitz, L.K., van Aardt, A.C., 2020. Late Quaternary palaeoenvironments in the central semi-arid region of South Africa from pollen in cave, pan, spring, stream and dung deposits. Quat. Int. https://doi.org/10.1016/j.quaint.2020.10.065.

Stockmarr, J., 1971. Tablets with spores used in absolute pollen analysis. Pollen Spores XIII, 615–621.

Street-Perrott, F.A., Perrott, R.A., 1993. Holocene vegetation, lake levels, and climate of africa. In: Wright, H.E., Kutzbach, J.E., Webb, T., Ruddiman, W.F., Street-Perrott, F. A., Bartlein, P.J. (Eds.), Global Climates since the Last Glacial Maximum. Chapter 13, pp. 318–356.

Taljaard, J.J., 1966. Atmospheric Circulation Systems, Synoptic Climatology and Weather Phenomena of South Africa. Part 6: Rainfall in South Africa. South African Weather Bureau. Technical paper 32 (100 pp).

Talma, A.S., Vogel, J.C., 1992. Late quaternary paleotemperatures derived from aspeleothem from Cango caves, Cape Province, South Africa. Quat. Res. 37 (2), 203–213.

Thackeray, J.F., 1987. Late Quaternary environmental changes inferred from small mammalian fauna, southern Africa. Clim. Chang. 10, 285–305.

Tyson, P.D., Preston-Whyte, R.A., 2000. The Weather and Climate of Southern Africa. Oxford University Press, Cape Town (396pp).

Valsecchi, V., Chase, B.M., Slingsby, J.A., Carr, A.S., Quick, L.J., Meadows, M.E., Cheddadi, R., Reimer, P.J., 2013. A high resolution 15,600-year pollen and microcharcoal record from the Cederberg Mountains, South Africa. Palaeogeogr. Palaeoclimatol. Palaeoecol. 387, 6–16.

Vogel, J.C., Fuls, A., Ellis, R.P., 1978. The geographical distribution of Kranz grasses in South Africa. S. Afr. J. Sci. 74, 209–215.

van Zinderen Bakker, E.M., 1976. The evolution of late Quaternary paleoclimates of Southern Africa. Palaeoecol. Africa 9, 160–202.